MATER. RES. LETT.
2025, VOL. 13, NO. 9, 917–927
https://doi.org/10.1080/21663831.2025.2531071

MATERIALS RESEARCH LETTERS
Taylor & Francis
Taylor & Francis Group

ORIGINAL REPORTS

Heterostructure enables new deformation mechanisms to enhance strength and work hardening

Bo Gao[a]*, Xinxin Dong[a]*, Xuefei Chen[a], Lirong Xiao[b], Qi Zhou[c], Xiaodong Han[d], Dongdi Yin[e], Hao Zhou[a] and Yuntian Zhu[a,f]

[a]Institute of Heterostructured Materials, Interdisciplinary Research Center, Liaoning Academy of Materials, Shenyang, People's Republic of China; [b]Nano and Heterogeneous Materials Center, School of Materials Science and Engineering, Nanjing University of Science and Technology, Nanjing, People's Republic of China; [c]Baidu AI Platform and Ecosystem, Baidu, Inc., Beijing, People's Republic of China; [d]Department of Materials Science & Engineering, Southern University of Science and Technology, Shenzhen, People's Republic of China; [e]Key Laboratory of Advanced Technologies of Materials, Ministry of Education, School of Materials Science and Engineering, Southwest Jiaotong University, Chengdu, People's Republic of China; [f]Department of Materials Science and Engineering, City University of Hong Kong, Hong Kong, People's Republic of China

ABSTRACT

Reflection of geometrically necessary dislocations (GNDs) has been reported effective in increasing strength and ductility of dual-phase alloys. However, this mechanism is rarely observed in conventional single-phase alloys. Here we report the activation of GND reflection by heterostructure in a single-phase steel, which produces high hetero-deformation induced (HDI) stress. Additionally, it promotes the formation of high-density immobile dislocation locks, which, together with HDI stress, produces high strain hardening. It appears that the condition for GND reflection is low stacking fault energy, high strength difference across hetero boundaries. These findings provide further guidance for designing heterostructures to achieve superior strain hardening.

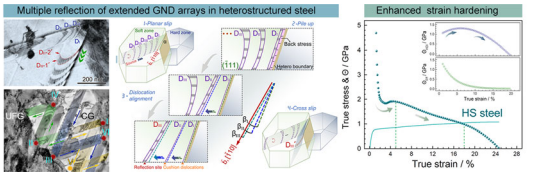

ARTICLE HISTORY
Received 6 June 2025

KEYWORDS
Heterostructured materials; geometrically necessary dislocations; dislocation reflection; cross slip; strain hardening

Introduction

Metallic materials have played a pivotal role in the progress of human civilization and technological advancements since the Bronze Age. The pursuit of strong and ductile metals remains a challenge, particularly in the face of escalating energy and environmental concerns. However, the inherent trade-off between strength and ductility has long been a Gordian knot in metallic structural materials, posing a formidable challenge for achieving both high strength and ductility. The primary strategy for improving the strength–ductility synergy is to sustain high strain-hardening [1–3]. To date, numerous attempts have been made to enhance strain hardening by tailoring composition and microstructure of metallic materials [4–8]. Typically, alloy compositions of high entropy alloys (HEAs) have been extensively explored to enhance strain hardening abilities by introducing additional deformation mechanisms such as stress-induced phase transformation and deformation twinning [9–11]. It is noted that the alloying strategy makes materials development more resource-dependent and progressively increases the overall production costs, having a negative impact on the long-term sustainability of high-performance metals [12]. Recently, the heterostructure

CONTACT Dongdi Yin ahnydd@swjtu.edu.cn Key Laboratory of Advanced Technologies of Materials, Ministry of Education, School of Materials Science and Engineering, Southwest Jiaotong University, Chengdu 610031, People's Republic of China; Hao Zhou hzhou@lam.ln.cn Institute of Heterostructured Materials, Interdisciplinary Research Center, Liaoning Academy of Materials, Shenyang 110167, People's Republic of China; Yuntian Zhu y.zhu@cityu.edu.hk Institute of Heterostructured Materials, Interdisciplinary Research Center, Liaoning Academy of Materials, Shenyang 110167, People's Republic of China Department of Materials Science and Engineering, City University of Hong Kong, Hong Kong 999077, People's Republic of China

*These authors contributed equally to this work.

Supplemental data for this article can be accessed online at https://doi.org/10.1080/21663831.2025.2531071.

architecture in metallic materials has garnered extensive attention because it offers an effective and economical method to conquer the strength–ductility paradox [13–16].

Heterostructured materials (HSMs) are a class of materials that are composed of heterogeneous zones with dramatically different (> 100%) mechanical or physical properties [17]. The interactive coupling between these heterogeneous zones produces a synergistic effect to help with obtaining mechanical properties superior to that of their homogeneous counterparts. The superiority in strength–ductility synergy of HSMs has been verified in various conventional metals with diverse heterostructure categories, such as heterogeneous lamellar structured Ti [18,19], laminate structured Cu/Cu-Zn alloy [20,21], harmonic structured Cu [22], gradient structured Al [23], etc. The outstanding mechanical properties of these HSMs originate from their heterostructure nature, which produces extra strengthening and strain hardening. Specifically, the HSMs strategy utilizes GNDs to produce strain hardening by inducing significant heterogeneous plastic deformation between different zones. Owing to the large difference in mechanical properties, large strain partitioning occurs between soft and hard zones, which produces strain gradient near zone boundaries. High-density GNDs are thereby generated to accommodate strain gradients. The pile-ups of GNDs produce long-range back stresses in soft zones and forward stresses in hard zones, collectively creating hetero-deformation induced (HDI) stress [24]. The kinematic evolution of HDI stress creates additional HDI strain hardening to increase the total strain hardening rate. Consequently, GNDs play a critical role in enhancing mechanical properties of HSMs.

The effect of GNDs primarily depends on their distribution and interactions with boundaries, such as grain boundaries and phase boundaries. When GNDs slip towards a boundary within a soft zone, one of the following scenarios may occur [25–28]: (1) piling up in front of the boundary, (2) being absorbed (pushed) into the boundary, (3) transmitting across the boundary, (4) being reflected from the boundary. The GND piling up against zone boundaries is the most effective way to produce back stress in soft zones, subsequently resulting in a high HDI stress [13]. However, the high stress concentration at the front of pileups could trigger the nucleation of cracks. In contrast, the GND absorption by or transmission across the hetero boundary aids in alleviating the local high stress, but negatively impacts the generation of back stress due to the saturation of GNDs in the pileup [28]. The desired scenario involves all GNDs emitted from Frank–Read dislocation source pile up to produce the back stress without the limitation by boundary failure. This can be realized by the GND reflection mechanism. When GND reflection occurs in soft zones, it not only mitigates stress concentration at the pileup front but also creates new dislocation pileups to multiply back stress [29]. In general, dual-phase structure facilitates the reflection of GNDs because of the difference in crystal structure and strength across the phase boundaries, which makes it hard for the GNDs in the soft zones to transmit. Conversely, dislocations tend to transmit across grain boundaries in the conventional single-phase metallic materials due to the same crystal structure and close strength across grain boundaries.

Therefore, it is required to tailor the composition and microstructure of single-phase metallic materials to activate GND reflection, thus enhancing strain hardening. The dislocation glide modes are influenced by the stacking fault energy (SFE). A Low SFE is helpful to promote planar slip and GND pileup [30,31]. However, perfect dislocations in metals with low SFEs tend to dissociate into extended dislocations, making it difficult for a dislocation to cross-slip [32]. Recent studies, particularly those employing molecular dynamics (MD) simulations, have extensively explored the cross-slip of extended dislocations, advancing our understanding of its mechanisms and guiding efforts to tailor microstructures that facilitate dislocation reflection [33–37]. The results reveal that cross-slip is a thermally activated process, with its rate determined by the activation barrier, which depends on various conditions, including obstacles to dislocation glide, and local stress around the dislocations [30,38]. Accordingly, the specific hetero boundaries and long-range internal stress in HSMs provide opportunities to motivate the cross-slip of extended dislocations. It might be possible to promote GND pileups and reflections through heterostructure architecture in low SFE materials.

Here we focus on a commercial 316L austenitic stainless steel with a low SFE of $\sim$ 26.5 mJ/m^2 which was measured by the regression formula proposed in Ref. [39]. A heterogeneous lamellar structure comprising ultrafine grains (UFG) and coarse grains (CG) layers was produced by cold rolling and partially recrystallization. *In-situ* transmission electron microscopy (TEM) straining tests were conducted to investigate the dislocation behavior during deformation. The detailed information on materials and methods can be found in the Supplementary materials. Multiple reflections of extended GNDs were observed near the hetero-boundaries between UFG and CG, which is different from the dislocation transmission commonly observed at conventional homogenous CG-CG boundaries in 316L steel. Specifically, the

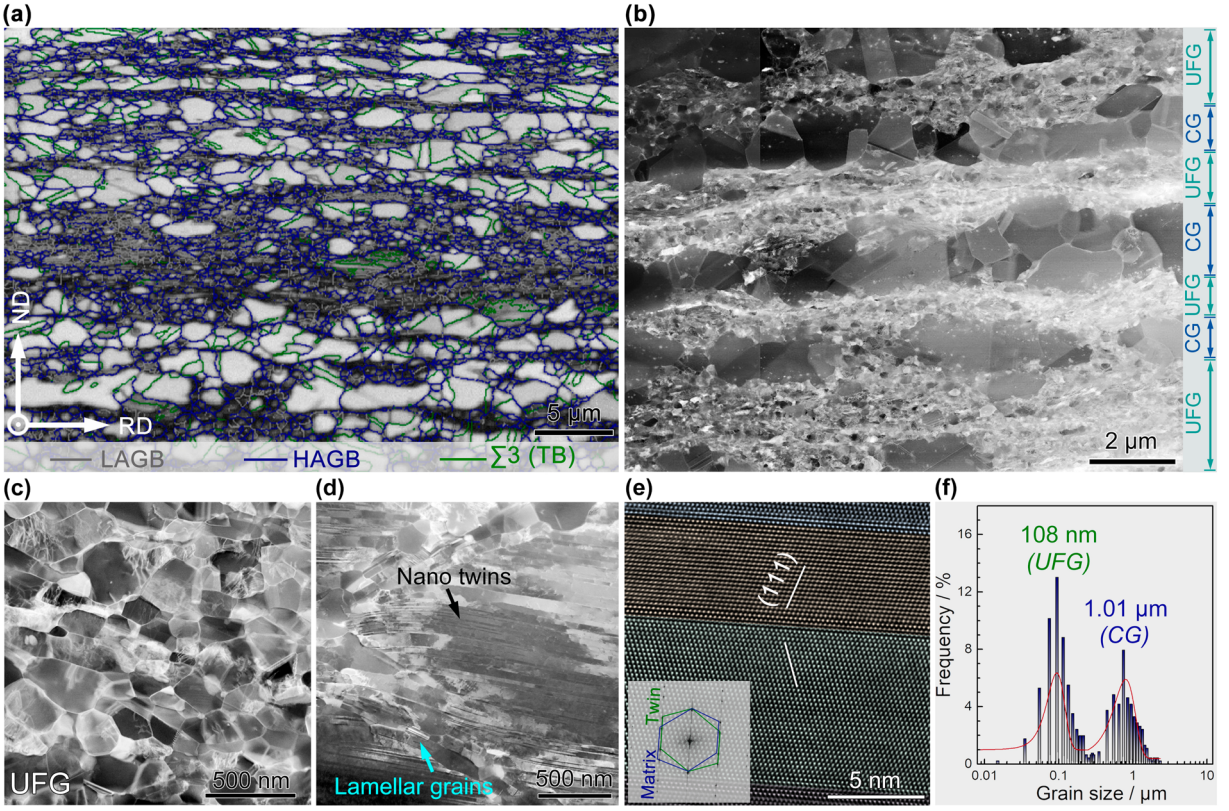

Figure 1. Microstructure of the HS 316L stainless steel. (a) Band contrast map of the HS steel, (b) HAADF-STEM image showing the distribution of CG and UFG lamella. (c) and (d) STEM images showing the ultrafine grains and nano twins in the UFG lamellae. (e) HRTEM of the nano twin. (f) Grain size distribution in the HS steel.

CG-UFG hetero-interfaces act as barriers and reflectors for GNDs. The reflection was directly induced by the cross-slip of extended dislocations. It appears that the heterostructure architecture in the present study can promote dislocation cross-slip, thus facilitating multiple dislocation reflection. The underlying mechanisms behind the multiple reflection of extended GNDs and its effects on mechanical properties are explored in detail.

Results and discussion

The inverse pole figure map of the as-received steel (Figure S1a) reveals a random texture and coarse grain (CG) structure, with an average grain size of $\sim 30\ \mu$m (Figure S1b). Cold rolling results in the formation of a refined lamellar structure (Figure S1c), accompanied by a diffraction pattern inset indicating the occurrence of stress-induced martensite transformation (SIMT). The deformed structure is characterized by ultrafine-grained lamellae and a high density of nano twins (Figure S1d and e). To produce the heterostructured (HS) steel, the cold-rolled sample was annealed at 760°C for 6 min. XRD analysis (Figure S2) confirms that most of the SIMT in the cold-rolled steel reversed to austenite during annealing.

Figure 1a shows the cross-sectional band contrast map of the HS steel, illustrating grain boundaries, including low-angle grain boundaries (LAGBs), high-angle grain boundaries (HAGBs), and Σ3 twin boundaries (TBs), typical of a heterogeneous lamellar structure composed of alternating CG and UFG lamellae induced by partial recrystallization [40,41]. TEM further reveals the substructures of the HS steel. Figure 1b shows that the CG lamellae consist of recrystallized grains with a low dislocation density, while the UFG lamellae are predominantly composed of equiaxed and lamellar grains (Figure 1c and d). There are some fine particles inside the coarse grains after annealing. The energy dispersive spectroscopy (EDS) results in Figure S3 indicate that these intragranular particles are rich in Cr and Mo, which are formed due to the local chemical segregation [42]. Moreover, nano-twins with a thickness of ~ 5 nm (Figure 1e) remain in the UFG lamella after annealing, due to their exceptional thermal stability [43]. The grain size distribution, shown in Figure 1f, reveals a bimodal pattern, with UFGs and CGs having average sizes of 108 nm and 1.01 μm, respectively. This bimodal distribution, along with variations in dislocation density, highlights the microstructural heterogeneity between the UFG and CG lamellae.

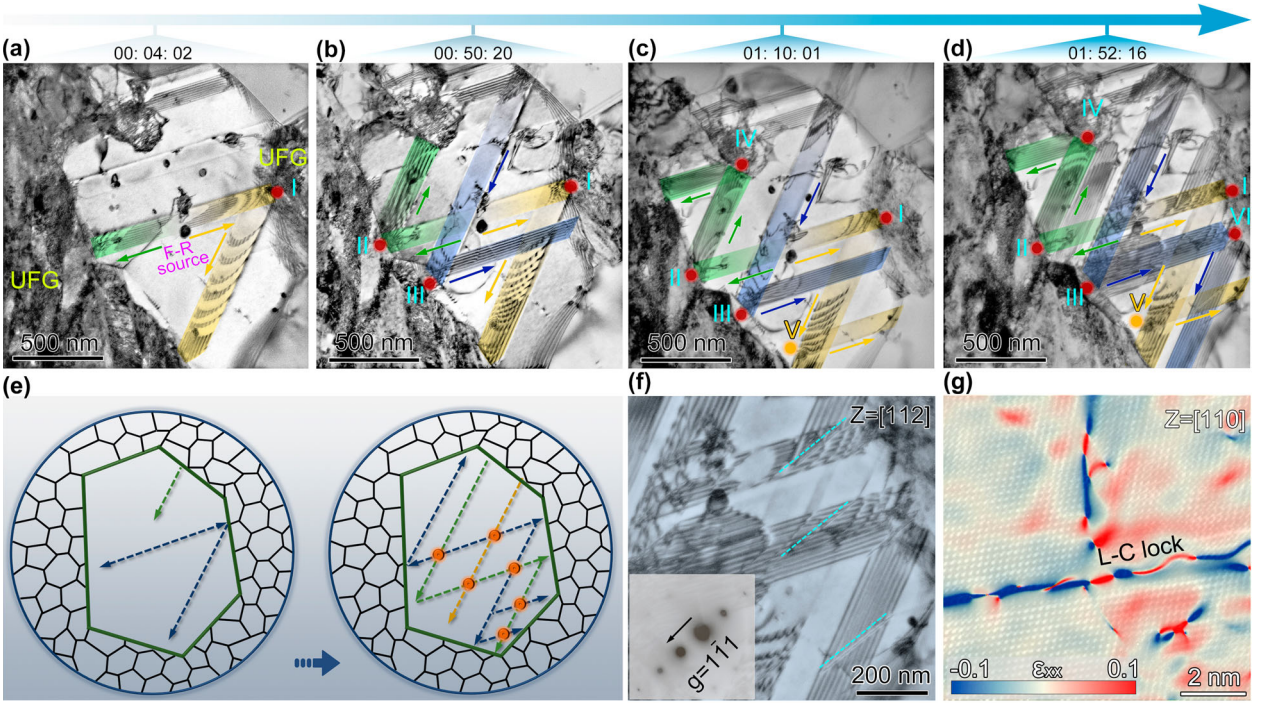

Figure 2. Multiple reflection of extended GNDs in the HS steel. (a)–(d) Snapshots from the Supplementary Movie 2 showing the multiple reflection of extended dislocations in the heterostructured steel. (e) Schematic illustrations showing the dislocation interactions due to multiple reflection. (f) Formation of high-density straight dislocations at the intersections induced by the multiple reflections. (g) HTERM image of the L–C lock overlapped with GPA map.

In-situ TEM straining tests provide valuable insights into the dynamic interactions between dislocations and grain boundaries [44,45]. The initial observations were performed on the homogeneous CG sample. Figure S4a-c, which are snapshots from Supplementary Movie 1, illustrate the dislocation motions in a 3-μm CG sample. Upon straining, dislocations are emitted from the grain boundary into grain interior, as indicated by the green arrow in Figure S4a. These dislocations are absorbed upon reaching the opposing grain boundary, leading to local stress concentrations. This stress is readily transmitted across the grain boundary, facilitating dislocation transmission [44]. Consequently, dislocations are pushed into and transmitted across the boundaries in the uniform CG sample, as marked by the blue arrows in Figure S4e.

In contrast, Figure 2a–d show close-up snapshots from the *in-situ* TEM video (Supplementary Movie 2), capturing the different dynamic interactions between dislocations and CG-UFG hetero boundaries in the HS steel. A Frank–Read (F–R) dislocation source within the CG emits GNDs along slip paths, highlighted in green and yellow. Upon encountering the hetero boundary at Position 'I', the dislocation array reflects into an intercepting slip plane, altering its pathway. As plastic deformation continues, additional reflections occur at Positions 'II' and 'III' (Figure 2b). With further straining, further reflections are observed at Positions 'IV' to 'VI', resulting in intersected zig-zag slip paths within the CG zone (Figure 2c and d).

The multiple reflections of dislocation arrays are thus facilitated in the soft zone of single-phase HS steel. It is noteworthy that reflection sites are not confined to hetero boundaries; they also occur at strong obstacles within the grain interior, such as at Position 'V'. In contrast to the relatively straightforward slip propagation within CG samples, where dislocation interactions are minimal at low strains, the zigzag pathways in HS steel promote complex interactions between dislocations from different slip planes, as shown in Figure 2e. High-density straight dislocations, marked by the dashed lines, are formed at the intersections induced by the multiple reflections of dislocation arrays (Figure 2f). The leading partial dislocations from two slip planes can interact to form immobile Lomer–Cottrell (L–C) locks [46,47]. When the observed direction is tilted from [112] to [110] zone axes, the HRTEM and corresponding GPA analysis (Figure 2g) were performed with the normal directions of $(00\bar{2})$ and $(\bar{2}20)$ planes being defined as x and y axes, respectively, as shown in Figure S5. It reveals the associated

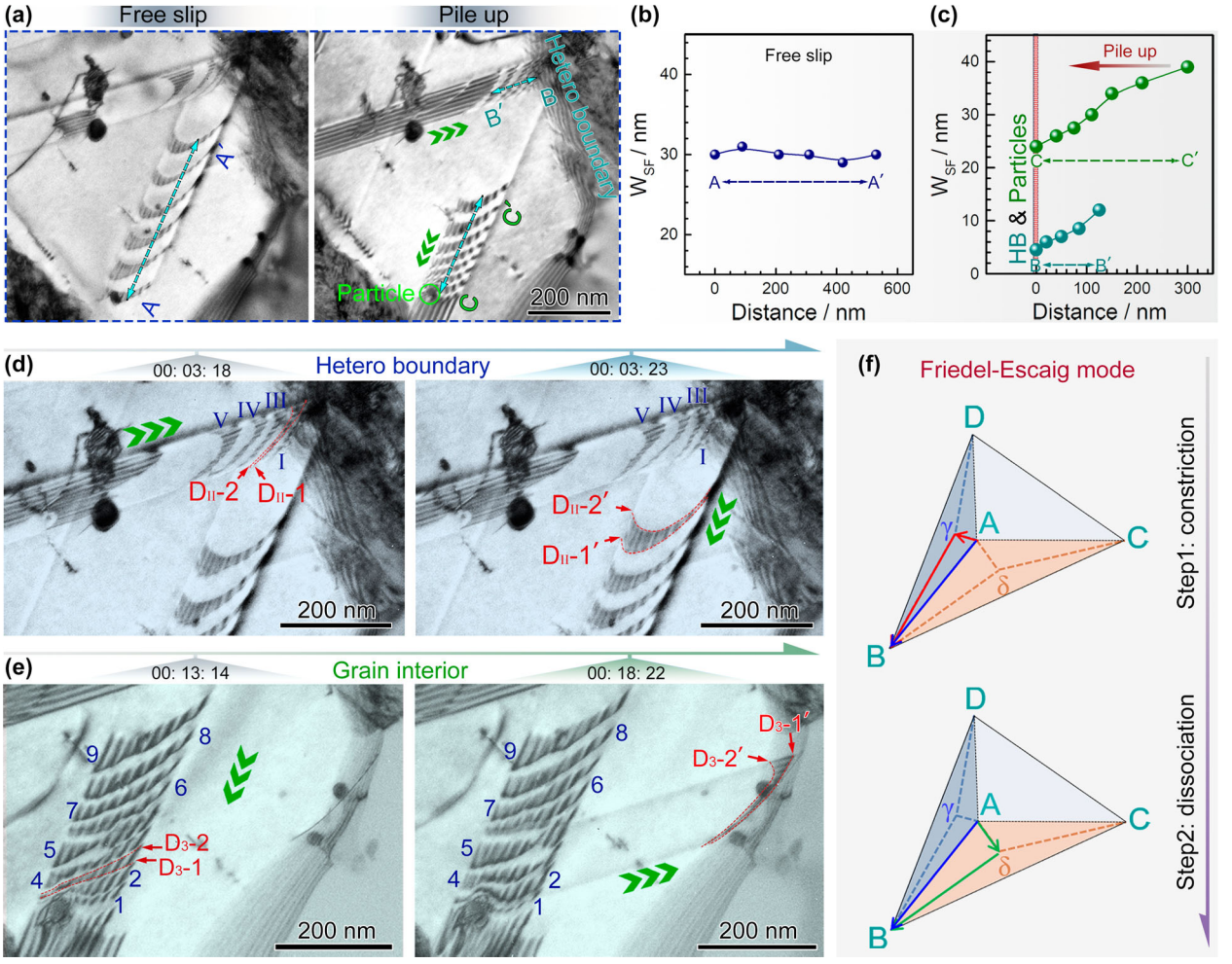

Figure 3. Cross-slip of extended dislocations in the HS steel. (a) Planar slip of extended dislocations in the CG zone. (b) and (c) Evolution of W_{SF} along the dislocation arrays when they free slip and pileup near obstacles (HB: hetero boundary). (d) Snapshots from the Supplementary Movie 3 showing the cross-slip near the CG-UFG hetero boundary. (e) Snapshots from the Supplementary Movie 4 showing the cross-slip inside the grain. (f) Dislocation reactions following FE cross-slip model.

lattice strain at the L–C lock, which impedes dislocation motion, thereby enhancing the mechanical properties of the HS steel.

The reflection of extended dislocation arrays is facilitated by cross-slip. Figure 3a shows planar slip of extended dislocations in the CG zone, where a low SFE promotes the dissociation of perfect dislocations into partials, which are separated by SF regions. The equilibrium width of the SF (W_{SF}) stabilizes at ~30 nm under free slip conditions, as shown in Figure 3b. However, W_{SF} dynamically evolves when extended dislocations accumulate near obstacles, such as hetero boundaries and intragranular particles. This results in a gradient distance along B-B' and C-C', narrowing to 4 and 24 nm near the hetero boundary and particles, respectively (Figure 3c), due to significant repulsive forces.

Although planar slip dominates due to the presence of SF regions, cross-slip can occur when the partial dislocations recombine into perfect dislocations by reducing W_{SF}. Sequential snapshots from Supplementary Movie 3 (Figure 3d) show the cross-slip near the CG-UFG hetero boundary. Five extended dislocation pairs encountering the CG-UFG boundary exhibit significant constriction of W_{SF}. Under strain, the second dislocation pair (D_{II}-1 and D_{II}-2) disappears from the original slip plane, while reappear as a new dislocation pair (D_{II}-1' and D_{II}-2') on the conjugate slip plane. Similarly, Supplementary Movie 4 (Figure 3e) captures cross-slip within the grain, where particle-induced repulsion compresses W_{SF}. With further straining, the third dislocation pair (D_3-1 and D_3-2) switches slip planes, with newly formed partial dislocations (D_3-1' and D_3-2') arriving at a grain boundary. These observations confirm that cross-slip involves both leading and trailing partials crossing to the conjugate slip plane via the Friedel-Escaig (FE) mechanism [38]. As illustrated in the Thompson tetrahedron (Figure 3f), the FE cross-slip process involves in the following two dislocation reactions: first, two partials ($\mathbf{A}\boldsymbol{\gamma}$ and $\boldsymbol{\gamma}\mathbf{B}$) converge

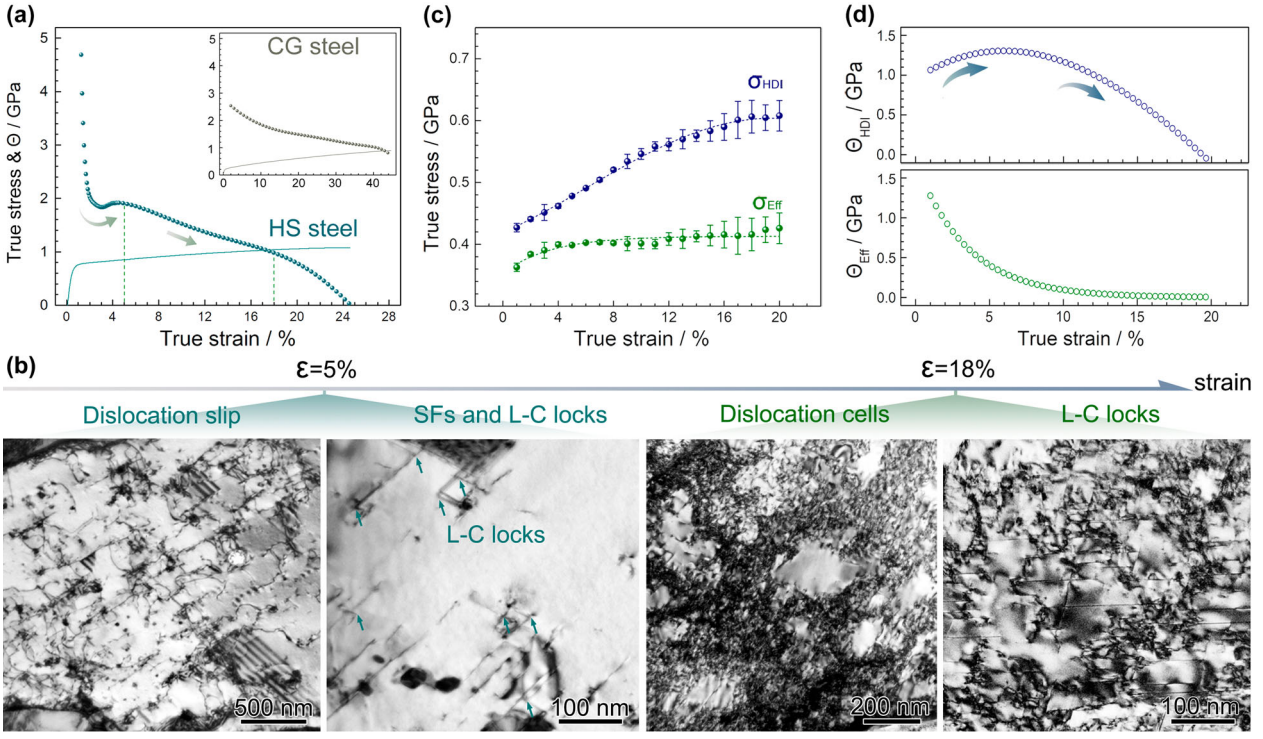

Figure 4. Strain hardening of the HS steel. (a) True stress–strain and strain hardening rate curves. (b) TEM micrographs of the deformed HS steel at strains of 5% and 18%. (c) σ_{HDI} and σ_{Eff} varying with applied strain. (d) Evolution of Θ_{HDI} and Θ_{Eff}.

into a screw dislocation **AB** (equation (1)), which then cross slips and dissociates into two new partials (**Aδ** and **δB**) in the conjugate plane (equation (2)).

$$\frac{a}{6}[\bar{1}2\bar{1}](\mathrm{A}\gamma) + \frac{a}{6}[\bar{2}11](\gamma\,\mathrm{B}) = \frac{a}{2}[\bar{1}10](\mathrm{AB}) \quad (1)$$

$$\frac{a}{2}[\bar{1}10](\mathrm{AB}) = \frac{a}{6}[\bar{1}2\bar{1}](\mathrm{A}\delta) + \frac{a}{6}[\bar{2}11](\delta\mathrm{B}) \quad (2)$$

Figure 4a shows the true stress and strain hardening rate ($\Theta_{Total} = d\sigma/d\varepsilon$) versus true strain curves of the HS steel, exhibiting a multi-stage strain hardening behavior. Initially, Θ_{Total} decreases before the strain of 2%, followed by a notable increase until the strain reaches 5%. Subsequently, Θ_{Total} decreases smoothly. In contrast, the strain hardening rate of the homogeneous CG sample monotonously decreases with strain, as shown in the inset. The upturn of strain hardening rate helps with postponing necking and improving ductility. This phenomenon is believed to be closely related to the microstructural evolution during deformation. The transformation induced plasticity (TRIP) and twinning induced plasticity (TWIP) effects typically contribute to the upturn of strain hardening rate in metastable austenitic steels and medium/high entropy alloys [48–50]. In the present study, additional interrupted tensile tests were carried out at strains of 5% and 18% to investigate the deformed microstructure. The EBSD phase maps at different strains are shown in Figure S6a to c. The martensitic content is rarely changed with tensile strain. In addition, the martensite distributed in the UFG zones is induced by the SIMT during cold rolling, rather than tensile deformation. TEM micrographs of the deformed samples are shown in Figure 4b. Notable planar slip and L–C locks are observed at the strain of 5%. At the strain of 18%, dislocation accumulations evolve into dense dislocation cells, along with the formation of higher density of L–C locks. No significant martensitic transformation and deformation twins are observed before the strain of 5%. Consequently, the upturn of strain hardening rate is primarily attributed to the heterostructure architecture.

HDI stress and hardening have been proved to promote an increase in the total strain hardening rate, which can be examined by cyclic loading-unloading-reloading tests [51–53]. The evolution of measured HDI stress (σ_{HDI}) and effective stress (σ_{Eff}) is shown in Figure 4c. Both the HDI and effective stresses increase with tensile strain. The magnitude of HDI hardening rate ($\Theta_{HDI} = d\sigma_{HDI}/d\varepsilon$) and forest strain hardening rate ($\Theta_{Eff} = d\sigma_{Eff}/d\varepsilon$) are deduced from the HDI and effective stress–strain curves [54]. As shown in Figure 4d, Θ_{HDI} increases first before the strain of 6% and then decreases, while Θ_{Eff} drops monotonously. It is noted that the increased Θ_{HDI} at the early deformation stage contributes to the upturn of Θ_{Total}, which has also been found in the heterogeneous lamellar structured Ti [18],

heterogeneous grain structured CrCoNi alloy [55], and gradient structured Cu-Al alloy [56].

In-situ TEM straining tests reveal the prevalent reflection of extended GNDs in the single-phase heterostructured 316L stainless steel, a phenomenon rarely observed in homogeneous materials. In homogeneous CG steel, dislocation absorption and transmission primarily occur at grain boundaries. However, in HS steel, extended GND arrays undergo multiple reflections within the soft zone near hetero boundaries, a behavior driven by cross-slip. While cross-slip of dissociated Shockley partials is generally constrained in low SFE materials, frequent cross-slip is observed in the studied heterostructured steel, governed by the FE model. It is of great significance to elucidate the cross-slip mechanisms in HS steel. The FE cross-slip process involves the constriction of Shockley partials followed by their re-dissociation. Overcoming the energy barrier for dislocation reactions needs a sufficient driving force [57]. Molecular dynamics and atomic calculations have predicted that cross-slip process is dependent on the applied shear stress [35,37,38,58]. The FE cross-slip requires sufficient Escaig stress acting on the edge component of the Shockley partial dislocations, which controls the distance between them [34,38]. Therefore, the prerequisite for cross-slip of extended dislocations is the driving force necessary for recombining the partial dislocations.

In the present study, the development of long-range internal stress within the heterostructure plays a pivotal role in enabling cross-slip. As illustrated in Figure 5a and b, dislocation sources within soft zones are activated under an applied resolved shear stress, emitting several GND pairs that pile up against the CG-UFG hetero boundary, which has an angle of (α) with the Burgers vector ($\vec{b}$) along [$\bar{1}$10]. The pile-up produces a stress concentration at the pile-up head, resulting in a gradient distribution of back stress (σ_{back}) within the soft zone, with the local stress near hetero boundaries exceeding that in grain interior. The σ_{back} near boundaries increases until stress relaxation happens through the plastic deformation of adjacent hard zones [59]. The σ_{back} contributes to sufficient Escaig stress required to narrow the width of SF, thereby enabling the constriction of partial dislocation.

The magnitude of long-range σ_{back} thereby plays a critical role in activating the multiple cross-slips. It correlates with the density of GND pile-ups ($\sigma_{back} \propto \rho_{pileup}$). ρ_{pileup} is significantly influenced by the strength contrast between the heterogeneous zones, which can be approximatively expressed as [60]:

$$\rho_{pileup} \approx \frac{4(\tau_{y,hard} - \tau_{y,soft})}{3\pi(1-\nu)(\tau_{y,soft} - \tau_0)l_{pileup}^2} \tag{3}$$

$$l_{pileup} \approx \frac{k_{HP}R^{3/2}}{\sqrt{2}MGb} \tag{4}$$

where $\tau_{y,hard}$ and $\tau_{y,soft}$ are the yield stress of hard and soft zones, τ_0 is the friction stress, l_{pileup} is the length of pile-ups against a hetero boundary, k_{HP} is the Hall–Petch constant, ν, R, M, G, b are Poisson's ratio, length of the pinning points of source, Taylor factor, shear modulus, and magnitude of burgers vector, respectively. In order to determine the k_{HP}, the homogenous samples with different grain sizes were obtained through annealing at 760°C with different times. Figure S7a shows the tensile curves of the homogeneous UFG and CG samples with average grain sizes of 120 nm and 1.15 μm, respectively, which are close to that of the hard and soft zones in the HS steel. As shown in Figure S7b, the grain size and yield strength of 316L stainless steel show a typical Hall–Petch relationship ($\tau_y = k_{HP}d^{-1/2}+\tau_0$), where the k_{HP} and τ_0 are calculated as 327 MPa·μm$^{-1/2}$, and 147 MPa, respectively. When describing $\tau_{y,soft}$ and$\tau_{y,hard}$ through the obtained Hall–Petch relationship, equation (3) can be deduced as following:

$$\rho_{pileup} \approx \frac{4(d_{hard}^{-1/2} - d_{soft}^{-1/2})}{3\pi(1-\nu)(d_{soft}^{-1/2})l_{pileup}^2} \tag{5}$$

Therefore, the ρ_{pileup} is determined by the average grain sizes of soft and hard zones (d_{soft} and d_{hard}) in the single-phase HS steel. Figure 5f shows the distribution map of the GND pile-up density (ρ_{pileup}) within the hard and soft zones ranging from 0.01 to 1 μm, and from 0.1 to 2 μm, respectively. Low ρ_{pileup} is required for the homogeneous structured steels during deformation. In contrast, large difference in d_{hard} and d_{soft} in HS sample leads to a larger strength contrast across the heterogeneous zones, necessitating more GND pileups to accommodate strain gradient near hetero boundaries. For example, in the HS1 steel (with $d_{hard} = 0.1$ μm and $d_{soft} = 1.0$ μm), ρ_{pileup} increases substantially to 0.68 μm^{-1}. As σ_{back} is proportional to ρ_{pileup}, this increase promotes the generation of back stress, thereby enhancing the driving force for the cross-slip of extended dislocations.

Cross-slip of extended dislocations predominately occur slightly away from the CG-UFG hetero boundaries or intragranular particles, rather than at sites of maximum local stress. This interesting phenomenon is related to dislocation configuration near obstacles, as schematically illustrated in Figure 5c and d. Upon piling up at the boundary, the leading GND (D_I) aligns its dislocation line with the boundary. Under the elevated back stress near the boundary, D_I recombines into a perfect dislocation. The recombined dislocation remains mixed-edged and screw character due to the angle of $\beta_I \approx \alpha$

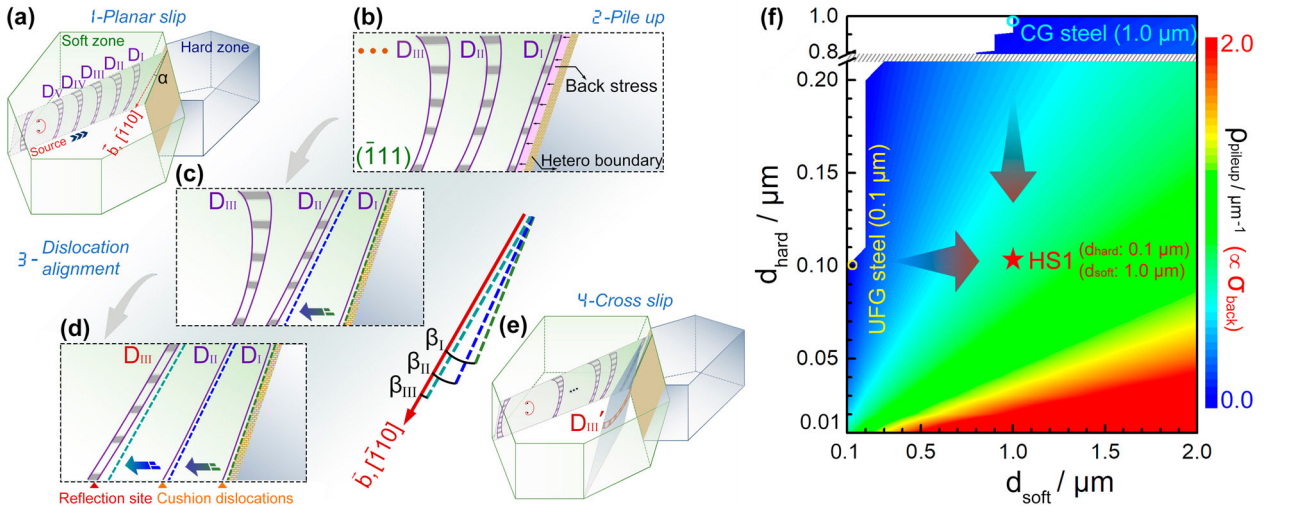

Figure 5. Cross-slip mechanism of extended dislocations in the HS steel. (a)–(e) Schematic illustration showing the cross-slip process of extended dislocations near hetero boundary. (f) ρ_{pileup} distribution map showing heterostructure promotes generation of high σ_{back} for recombining partials.

between the Burgers vector and the boundary, thus preventing cross-slip. This behavior is verified in Figure S8, where constricted dislocations remain on their original slip plane. For perfect dislocations to undergo cross-slip, their dislocation lines must align parallel to their Burgers vector. The leading GNDs in the pile-up (D_I and D_{II}) exert an expelling force on the incoming dislocation (D_{III}), acting as a cushion to gradually align its segments (Figure 5d). As a result, the angles between dislocation lines and $\vec{b}$ reduce from β_I to β_{II} and β_{III}. Once D_{III} aligns with its dislocation segment parallel to $\vec{b}$ ($\beta_{III} = 0$), it can cross-slip after recombined into a perfect screw dislocation. This screw dislocation subsequently dissociates into two new Shockley partials (D_{III}') in the cross-slip plane (Figure 5e). Therefore, the essential conditions for cross-slip of extended dislocations involve the generation of substantial long-range internal stress to constrict the stacking fault and the alignment of dislocation lines near obstacles, ensuring local recombination and enable efficient cross-slip.

The multiple reflection has significant influences on accommodating plastic deformation and improving mechanical properties of HS steel. First, this strategy is effective in suppressing strain localization. The cross-slip process transfers dislocations from a single slip plane to multiple ones, allowing stress concentrations to be redistributed and create evenly distributed dislocation within grains [61]. The frequent cross-slip in the HS steel enhances the efficiency of slip transmissibility, thus promoting stress transfer so as to suppress strain localization [6,62]. It is evidenced that strain delocalization in the heterostructured materials help with stabilizing plastic deformation and improving ductility [63]. Second, the multiple cross-slip occurred in the HS steel enhances strain hardening rate. Generally, cross-slip plays a dual role in strain hardening. It reduces the strain hardening rate at the large-strain stage because it results in dynamic recovery by enabling the mutual annihilation of dislocations and allowing them to escape from pile-ups [64]. Conversely, it can promote work hardening by forming stable dislocation structures in the low-strain stage [65,66]. In this work, the multiple cross-slip in this HS steel help with improving strain hardening from the following two aspects. On one hand, dislocation reflection prevents the absorption of GNDs by boundaries and multiply the GND pile-ups, thus enhancing HDI stress and hardening [28]. According to the calculation using equation (5), the ρ_{pileup} should be 0.68 μm^{-1} in the HS steel. It indicates that in a one-dimension simplified configuration, on average a GND pile-up is needed every 1.5 μm to accommodate the heterogeneous deformation. Actually, the ρ_{pileup} estimated from the in-situ staining tests (Figure 2) can reach up to $\sim$3.5 μm^{-1}, which is induced by the multiple reflection of GND arrays. As evidenced in Figure 4c and d, HDI stress and Θ_{HDI} increase faster before the strain of 6%, which is primarily attributed to the prevailing GND pileups. On the other hand, multiple cross-slip fabricates stable dislocation structures, i.e. L–C locks, which effectively hinder dislocation motion to enhance the strain hardening rate.

Since the multiple reflections of extended dislocations can enhance the strain hardening ability of the HS steel. It is desired to take full advantage of this mechanism via alloy composition design and microstructure architecture. First, low SFE is required to realize the planar slip of extended dislocations, thus producing effective pileups

[67,68]. Second, in order to activate multiple cross-slip of extended dislocations, high local stress around dislocations is required. Therefore, it is expected to introduce sufficient stable obstructions to dislocation glide. In this work, the hetero boundary (CG-UFG boundary) was employed. Note that a large strength contrast between the soft zones and hard zones is demanded to reinforce the effectiveness of hetero boundaries. For instance, the YS of hard zones in the HS steel is about triple that of soft zones. As the soft zones begins to deformation plastically, the neighboring hard zones retain elastic state. This notable mechanical incompatibility enhances local internal stress in the embedded soft zone to a high level, enabling the occurrence of cross-slip. Besides of the hetero boundaries in this study, the stable structures, such as dislocation locks, dislocation jogs, precipitations are also effective in hindering dislocation motion to facilitate cross-slip [69–71]. Third, the soft zones are proposed to be surrounded by hard zones, providing sufficient hetero boundaries for reflection. If a large number of soft zones is connected by CG-CG boundaries, the stress is proponed to be relaxed by the propagating plastic flow across the boundaries and the dislocation reflections will be suppressed.

Summary

In conclusion, multiple reflection of extended GNDs in the soft zone is implemented in a single-phase heterostructured 316L stainless steel, which is induced by the boosted cross-slip of extended dislocations following the Friedel-Escaig model. In order to achieve this, large long-range internal stress is required to realize the local constriction of SFs within extended dislocations. Additionally, the cushioning dislocations near the obstacles are necessary to help with aligning the incoming dislocation lines for completing cross-slip. The multiple reflection of dislocations has positive influences on the strain hardening and mechanical properties of metallic materials. First, it is capable to inhibit strain localization through effective slip and stress transfer. Second, the multiple reflection of dislocations emitted from one dislocation source produce effective HDI hardening. Third, the multiple reflection of extended dislocations promotes the formation of high-density L–C locks, significantly enhancing the strain hardening rate of the HS steel. These findings highlight the potential of heterostructures to overcome the traditional strength–ductility trade-off.

Disclosure statement

No potential conflict of interest was reported by the author(s).

Funding

This work was supported by the National Key R&D Program of China (grant number 2021YFA1200201), the National Natural Science Foundation of China (grant numbers 52201124, 52401153, and 52171118), the Natural Science Foundation of Jiangsu Province (grant number BK20220960), Heilongjiang Provincial Natural Science Foundation of China (grant number LH2023E112).

ORCID

Dongdi Yin http://orcid.org/0000-0002-0078-1244

References

[1] Zhu YT, Wu XL. Ductility and plasticity of nanostructured metals: differences and issues. Mater Today Nano. 2018;2:15–20. doi:10.1016/j.mtnano.2018.09.004
[2] Valiev RZ, Estrin Y, Horita Z, et al. Fundamentals of superior properties in bulk nanoSPD materials. Mater Res Lett. 2016;4(1):1–21. doi:10.1080/21663831.2015.1060543
[3] Dong XX, Shen YF, Zhu YT. Moderating strain hardening rate to produce high ductility and high strength in a medium carbon TRIP steel. Mater Res Lett. 2023;11(1):69–75. doi:10.1080/21663831.2022.2116295
[4] Ding Q, Zhang Y, Chen X, et al. Tuning element distribution, structure and properties by composition in high-entropy alloys. Nature. 2019;574(7777):223–227. doi:10.1038/s41586-019-1617-1
[5] Liu L, Yu Q, Wang Z, et al. Making ultrastrong steel tough by grain-boundary delamination. Science. 2020;368(6497):1347–1352. doi:10.1126/science.aba9413
[6] Wu H, Fan G. An overview of tailoring strain delocalization for strength-ductility synergy. Prog Mater Sci. 2020;113:100675. doi:10.1016/j.pmatsci.2020.100675
[7] Xie A, Huan Y, Xiaoyu B, et al. Formation mechanism of cellular structure of Ni32.5Co15Cr10Fe23Al17.5Mo1.5W0.5 eutectic high-entropy alloys by selective laser melting. Mater Res Lett. 2025;13(3):274–281. doi:10.1080/21663831.2024.2443051
[8] Gorsse S, Dorian H, Stéphane G, et al. Contributions and role of B2 nanoparticles in the exceptional strength/ductility trade-offs of Al0.3CoCrFeMnNi high entropy alloy. Mater Res Lett. 2025;13(4):420–428. doi:10.1080/21663831.2025.2466779
[9] Yang G, Kim JK. Hierarchical precipitates, sequential deformation-induced phase transformation, and enhanced back stress strengthening of the micro-alloyed high entropy alloy. Acta Mater. 2022;233:117974. doi:10.1016/j.actamat.2022.117974
[10] Li Z, Pradeep KG, Deng Y, et al. Metastable high-entropy dual-phase alloys overcome the strength–ductility trade-off. Nature. 2016;534(7606):227–230. doi:10.1038/nature17981
[11] Geng Z, Zhongliang S, Chao C, et al. Co-existence of nanoprecipitates with solute nitrogen evades the strength-ductility trade-off in metastable high entropy alloy. Mater Res Lett. 2024;12(6):433–441. doi:10.1080/21663831.2024.2340637
[12] Li X, Lu K. Playing with defects in metals. Nat Mater. 2017;16(7):700–701. doi:10.1038/nmat4929

[13] Zhu Y, Wu X. Heterostructured materials. Prog Mater Sci. 2023;131:101019. doi:10.1016/j.pmatsci.2022.101019
[14] Zhu Y. Introduction to heterostructured materials: A fast emerging field. Metall Mater Trans A. 2021;52(11): 4715–4726. doi:10.1007/s11661-021-06438-8
[15] Gao B, Lai Q, Cao Y, et al. Ultrastrong low-carbon nanosteel produced by heterostructure and interstitial mediated warm rolling. Sci Adv. 2020;6(39):eaba8169. doi:10.1126/sciadv.aba8169
[16] Li T, Haiyang C, Yubo H, et al. Enhanced strength and ductility in (CoCrNi)92Mo2Al6 medium entropy alloy via dual heterogeneous structures. Mater Res Lett. 2024;12(12):895–902. doi:10.1080/21663831.2024.2399579
[17] Dong X, Gao B, Xiao L, et al. Heterostructured metallic structural materials: research methods, properties, and future perspectives. Adv Func Mater. 2024;34(51):2410521. doi:10.1002/adfm.202410521
[18] Wu X, Yang M, Yuan F, et al. Heterogeneous lamella structure unites ultrafine-grain strength with coarse-grain ductility. Proc Natl Acad Sci U S A. 2015;112(47): 14501–14505. doi:10.1073/pnas.1517193112
[19] Wu D, Hao M, Zhang T, et al. Heterostructures enhance simultaneously strength and ductility of a commercial titanium alloy. Acta Mater. 2023;257:119182. doi:10.1016/j.actamat.2023.119182
[20] Huang CX, Wang YF, Ma XL, et al. Interface affected zone for optimal strength and ductility in heterogeneous laminate. Mater Today. 2018;21(7):713–719. doi:10.1016/j.mattod.2018.03.006
[21] Ma X, Huang C, Moering J, et al. Mechanical properties of copper/bronze laminates: role of interfaces. Acta Mater. 2016;116:43–52. doi:10.1016/j.actamat.2016.06.023
[22] Li G, Jiang J, Ma H, et al. Superior strength–ductility synergy in three-dimensional heterogeneous-nanostructured metals. Acta Mater. 2023;256:119143. doi:10.1016/j.actamat.2023.119143
[23] Wang F, Yue L, Xinren C, et al. Superior strength–ductility combination in Al alloys via dislocation gradient structure. Mater Res Lett. 2023;11(5):347–353. doi:10.1080/21663831.2022.2151851
[24] Zhu Y, Wu X. Perspective on hetero-deformation induced (HDI) hardening and back stress. Mater Res Lett. 2019;7(10):393–398. doi:10.1080/21663831.2019.1616331
[25] Wang J. Atomistic simulations of dislocation pileup: grain boundaries interaction. JOM. 2015;67(7):1515–1525. doi:10.1007/s11837-015-1454-0
[26] Shen Z, Wagoner RH, Clark WAT. Dislocation and grain boundary interactions in metals. Acta Metall. 1988;36(12):3231–3242. doi:10.1016/0001-6160(88)90058-2
[27] Shen Z, Wagoner RH, Clark WAT. Dislocation pile-up and grain boundary interactions in 304 stainless steel. Scripta Metall. 1986;20(6):921–926. doi:10.1016/0036-9748(86)90467-9
[28] Zhou H, Huang C, Sha X, et al. In-situobservation of dislocation dynamics near heterostructured interfaces. Mater Res Lett. 2019;7(9):376–382. doi:10.1080/21663831.2019.1616330
[29] Liu Y, Xu M, Xiao L, et al. Dislocation array reflection enhances strain hardening of a dual-phase heterostructured high-entropy alloy. Mater Res Lett. 2023;11(8):638–647. doi:10.1080/21663831.2023.2208166
[30] He F, Wei S, Cann JL, et al. Composition-dependent slip planarity in mechanically-stable face centered cubic complex concentrated alloys and its mechanical effects. Acta Mater. 2021;220:117314. doi:10.1016/j.actamat.2021.117314
[31] An D, Xiao Y, Yu J, et al. The role of dislocation type in the thermal stability of cellular structures in additively manufactured austenitic stainless steel. Adv Sci. 2024;11(33):2402962. doi:10.1002/advs.202402962
[32] Hull D, Bacon DJ. Introduction to dislocations. Amsterdam: Elsevier Science; 2011.
[33] Oren E, Yahel E, Makov G. Kinetics of dislocation cross-slip: a molecular dynamics study. Comput Mater Sci. 2017;138:246–254. doi:10.1016/j.commatsci.2017.06.039
[34] Esteban-Manzanares G, Santos-Güemes R, Papadimitriou I, et al. Influence of the stress state on the cross-slip free energy barrier in Al: An atomistic investigation. Acta Mater. 2020;184:109–119. doi:10.1016/j.actamat.2019.10.055
[35] Xu S, Xiong L, Chen Y, et al. Shear stress- and line length-dependent screw dislocation cross-slip in FCC Ni. Acta Mater. 2017;122:412–419. doi:10.1016/j.actamat.2016.10.005
[36] Hussein AM, Rao SI, Uchic MD, et al. Microstructurally based cross-slip mechanisms and their effects on dislocation microstructure evolution in FCC crystals. Acta Mater. 2015;85:180–190. doi:10.1016/j.actamat.2014.10.067
[37] Kang K, Yin J, Cai W. Stress dependence of cross slip energy barrier for face-centered cubic nickel. J Mech Phys Solids. 2014;62:181–193. doi:10.1016/j.jmps.2013.09.023
[38] Kuykendall WP, Wang Y, Cai W. Stress effects on the energy barrier and mechanisms of cross-slip in FCC nickel. J Mech Phys Solids. 2020;144:104105. doi:10.1016/j.jmps.2020.104105
[39] Meric de Bellefon G, van Duysen JC, Sridharan K. Composition-dependence of stacking fault energy in austenitic stainless steels through linear regression with random intercepts. J Nucl Mater. 2017;492:227–230. doi:10.1016/j.jnucmat.2017.05.037
[40] Li J, Fang C, Liu Y, et al. Deformation mechanisms of 304L stainless steel with heterogeneous lamella structure. Mater Sci Eng A. 2019;742:409–413. doi:10.1016/j.msea.2018.11.047
[41] Li J, Cao Y, Gao B, et al. Superior strength and ductility of 316L stainless steel with heterogeneous lamella structure. J Mater Sci. 2018;53(14):10442–10456. doi:10.1007/s10853-018-2322-4
[42] Lescur A, Stergar E, Lim J, et al. Microstructural investigation and identification of intermetallic σ-phase in solution annealed 316L-type austenitic stainless steel. Mater Charact. 2021;182:111524. doi:10.1016/j.matchar.2021.111524
[43] Lu K. Stabilizing nanostructures in metals using grain and twin boundary architectures. Nat Rev Mater. 2016;1(5): 16019. doi:10.1038/natrevmats.2016.19
[44] Gao B, Wang L, Liu Y, et al. In-situ TEM investigation on deformation mechanisms of a fine-grained 316L stainless steel. Scripta Mater. 2023;234:115538. doi:10.1016/j.scriptamat.2023.115538

[45] Wang L, Zhang Y, Zeng Z, et al. Tracking the sliding of grain boundaries at the atomic scale. Science. 2022;375(6586):1261–1265. doi:10.1126/science.abm2612
[46] Xu XD, Liu P, Tang Z, et al. Transmission electron microscopy characterization of dislocation structure in a face-centered cubic high-entropy alloy Al0.1CoCrFeNi. Acta Mater. 2018;144:107–115. doi:10.1016/j.actamat.2017.10.050
[47] Li Z, Cui Y, Yan W, et al. Enhanced strengthening and hardening via self-stabilized dislocation network in additively manufactured metals. Mater Today. 2021;50:79–88. doi:10.1016/j.mattod.2021.06.002
[48] Vázquez-Fernández NI, Nyyssönen T, Isakov M, et al. Uncoupling the effects of strain rate and adiabatic heating on strain induced martensitic phase transformations in a metastable austenitic steel. Acta Mater. 2019;176:134–144. doi:10.1016/j.actamat.2019.06.053
[49] Pei Z, Rozman KA, Doğan ÖN, et al. Machine-Learning microstructure for inverse material design. Adv Sci. 2021;8(23):2101207. doi:10.1002/advs.202101207
[50] Ding C, Gang N, Zhihui Z, et al. Enhancing strength and ductility in heterolamellar medium-Mn steel through bamboo-like microstructure design. Mater Res Lett. 2024;12(11):843–851. doi:10.1080/21663831.2024.2394575
[51] Gao B, Wang L, Liu Y, et al. Enhanced strength and ductility of the low-carbon steel with heterogeneous lamellar dual-phase structure produced by cyclic intercritical rolling. J Mate Res Technol. 2023;23:6230–6243. doi:10.1016/j.jmrt.2023.02.214
[52] Gao B, Liu Y, Chen X, et al. Heterogeneous plastic deformation and HDI strengthening of the heterostructured dual-phase steels investigated by in-situ SEM-DIC. Mater Sci Eng A. 2024;893:146149. doi:10.1016/j.msea.2024.146149
[53] Cheng Q, Bo Y, Chao Z, et al. Optimizing strength-ductility synergy in lightweight steel via heterogeneous design: discontinuous fibrous ferrite. Mater Res Lett. 2024;12(12):947–955. doi:10.1080/21663831.2024.2406913
[54] Yang MX, Yuan FP, Xie QG, et al. Strain hardening in Fe–16Mn–10Al–0.86C–5Ni high specific strength steel. Acta Mater. 2016;109:213–222. doi:10.1016/j.actamat.2016.02.044
[55] Wang Y, Ma X, Guo F, et al. Strong and ductile CrCoNi medium-entropy alloy via dispersed heterostructure. Mater Des. 2023;225:111593. doi:10.1016/j.matdes.2023.111593
[56] Liu H, Gao B, Yang Y, et al. Strain hardening behavior and microstructure evolution of gradient-structured Cu-Al alloys with low stack fault energy. J Mater Res Technol. 2022;19:220–229. doi:10.1016/j.jmrt.2022.05.027
[57] Shen S, Xie P, Wu C, et al. Cross-slip of extended dislocations and secondary deformation twinning in a high-Mn TWIP steel. Inter J Plast. 2024;175:103922. doi:10.1016/j.ijplas.2024.103922
[58] Rao SI, Dimiduk DM, El-Awady JA, et al. Activated states for cross-slip at screw dislocation intersections in face-centered cubic nickel and copper via atomistic simulation. Acta Mater. 2010;58(17):5547–5557. doi:10.1016/j.actamat.2010.06.005
[59] Wang Y, Huang C, Ma X, et al. The optimum grain size for strength-ductility combination in metals. Inter J Plast. 2023;164:103574. doi:10.1016/j.ijplas.2023.103574
[60] Li J, Ma X, Lu K, et al. Unusual deformation mechanisms evoked by hetero-zone interaction in a heterostructured FCC high-entropy alloy. Acta Mater. 2025;282:120516. doi:10.1016/j.actamat.2024.120516
[61] Kim SD, Park JY, Park SJ, et al. Direct observation of dislocation plasticity in high-Mn lightweight steel by in-situ TEM. Sci Rep. 2019;9(1):15171. doi:10.1038/s41598-019-51586-y
[62] Bitzek E, Brandl C, Derlet PM, et al. Dislocation cross-slip in nanocrystalline FCC metals. Phys Rev Lett. 2008;100(23):235501. doi:10.1103/PhysRevLett.100.235501
[63] Liu Y, Cao Y, Mao Q, et al. Critical microstructures and defects in heterostructured materials and their effects on mechanical properties. Acta Mater. 2020;189:129–144. doi:10.1016/j.actamat.2020.03.001
[64] Patil CS, Chakraborty S, Niezgoda SR. Cross slip based dynamic recovery during plane strain compression of aluminium and its role in preferential nucleation of the cube-oriented recrystallized grains. Acta Mater. 2024;272:119913. doi:10.1016/j.actamat.2024.119913
[65] Das SR, Shyamal S, Sahu T, et al. On the mechanism of cross-slip induced dislocation substructure formation in an high-Mn steel. Materialia. 2021;15:101042. doi:10.1016/j.mtla.2021.101042
[66] Jackson PJ. The role of cross-slip in the plastic deformation of crystals. Mater Sci Eng. 1983;57(1):39–47. doi:10.1016/0025-5416(83)90025-3
[67] Mililitsky M, De Wispelaere N, Petrov R, et al. Characterization of the mechanical properties of low-nickel austenitic stainless steels. Mater Sci Eng A. 2008;498(1):289–295. doi:10.1016/j.msea.2008.08.012
[68] Hong SI, Laird C. Mechanisms of slip mode modification in F.C.C. solid solutions. Acta Metall. 1990;38(8):1581–1594. doi:10.1016/0956-7151(90)90126-2
[69] Tirunilai AS, Weiss KP, Freudenberger J, et al. Revealing the role of cross slip for serrated plastic deformation in concentrated solid solutions at cryogenic temperatures. Metals (Basel). 2022;12(3):514. doi:10.3390/met12030514
[70] Chen D, Costello LL, Geller CB, et al. Atomistic modeling of dislocation cross-slip in nickel using free-end nudged elastic band method. Acta Mater. 2019;168:436–447. doi:10.1016/j.actamat.2019.02.035
[71] Singh CV, Mateos AJ, Warner DH. Atomistic simulations of dislocation–precipitate interactions emphasize importance of cross-slip. Scripta Mater. 2011;64(5):398–401. doi:10.1016/j.scriptamat.2010.10.041